OPEN

Distinct modes of perimembrane TRP channel turnover revealed by TIR-FRAP

Debapriya Ghosh, Andrei Segal & Thomas Voets

Laboratory of Ion Channel Research and TRP channel Research Platform Leuven (TRPLe) Department of Cellular and Molecular Medicine, KU Leuven, Belgium.

Transient Receptor Potential (TRP) channels form a broadly expressed and functionally diverse family of cation channels involved in various (patho)physiological processes. Whereas the mechanisms that control opening of TRP channels have been extensively studied, little is known about the transport processes of TRP channels to and within the plasma membrane. Here we used Total Internal Reflection - Fluorescence Recovery after Photobleaching (TIR-FRAP) to selectively visualize and bleach the fluorescently labeled TRP channels TRPV2 and TRPM4 in close proximity of the glass-plasma membrane interface, allowing detailed analysis of their perimembrane dynamics. We show that recovery of TRPM4 occurs via 200-nm diameter transport vesicles, and demonstrate the full fusion of such vesicles with the plasma membrane. In contrast, TRPV2 recovery proceeded mainly via lateral diffusion from non-bleached areas of the plasma membrane. Analysis of the two-dimensional channel diffusion kinetics yielded 2D diffusion coefficients ranging between 0.1 and 0.3 μm^2/s, suggesting that these TRP channels move relatively unrestricted within the plasma membrane. These data demonstrate distinct modes of TRP channel turnover at the plasma membrane and illustrate the usefulness of TIR-FRAP to monitor these processes with high resolution.

Transient Receptor Potential (TRP) channels form a superfamily of ubiquitously expressed and functionally diverse cation permeable channels[1,2]. TRP channels function as cellular sensors that play key roles in various sensory and homeostasic processes in mammals, such as somatosensation, taste, cardiovascular function, cation (re)absorption and glucose homeostasis[1–5]. In contrast to the large body of research that has been conducted unraveling activation mechanisms and (patho)physiological functions of TRP, very little is known about the cellular trafficking mechanisms that determine TRP channel abundance at the plasma membrane, and the actual process of TRP channel incorporation into the plasma membrane has not yet been visualized[6–8]. Nevertheless, dynamic changes in the availability of TRP channels at the plasma membrane have been put forward as potentially important regulatory mechanisms of TRP channel function *in vivo*[9–13].

By creating an evanescent wave whose intensity decays exponentially with distance from the glass coverslip, Total Internal Reflection Fluorescence (TIRF) microscopy allows selective visualisation of fluorophores within ~100–200 nm from the plasma membrane[14–16]. Whereas some earlier studies have used TIRF microscopy to describe near-membrane TRP channel trafficking[9,11,13,17], detailed visualization of the process of TRP channel incorporation and lateral diffusion at the plasma membrane is lacking. Interestingly, the evanescent wave can also be used to selectively bleach fluorophores in close proximity of the glass coverslip and follow their recovery, a technique called TIR-FRAP. TIR-FRAP enables visualization of only the incoming fluorescence after bleaching of all resident fluorescence from the membrane and near-membrane zone, which allows unparalleled clarity of near-membrane trafficking events[18,19].

Here, we applied for the first time TIR-FRAP for quantitative investigation of TRP channel dynamics at the plasma membrane. We focused on two TRP channels, TRPM4, and TRPV2, for which earlier research suggested that membrane trafficking represents an important regulatory mechanism. Membrane incorporation and endocytosis of TRPM4 has been put forward as a major regulatory mechanism in pancreatic β−cells[10], vascular smooth muscle cells[20] and human Purkinje fibers[21]. Rapid membrane incorporation in response to chemical and mechanical stimuli was reported to act as a key regulator of TRPV2 functionality in various cell types[22,23]. Our present results indicate distinct modes of TRP channel turnover at the plasma membrane of HEK293 cells, and provide the first details of the membrane incorporation and lateral diffusion of these TRP channels.

Results

Visualization of TRPV2 and TRPM4 at the plasma membrane. To monitor the perimembrane dynamics of TRPV2 and TRPM4, we coupled GFP at their C termini and expressed the constructs in HEK293 cells.

Visualization using TIRF microscopy, using an evanescent field declining e-fold in 80 nm (Fig. 1a top) revealed extensive perimembrane fluorescence in both TRPV2 and TRPM4 transfected cells (pre-bleach panels in Figs. 1b,c and 2a,b; Supplementary Figure S1). At various time points after transfection, TRPV2-GFP was consistently observed as static fluorescence that evenly covered the entire footprint of the cell at the glass coverslip (Supplementary movie S1; Supplementary Figure S1). In the case of TRPM4-GFP, a similar homogenous distribution was found, but, additionally, highly motile punctate structures were regularly observed (Supplementary movie S2; Supplementary Figure S1), in line with an earlier report[20]. For both channels, the extensive perimembrane staining observed using TIRF microscopy prevented a detailed analysis of TRP channel dynamics and turnover at the membrane.

We therefore used TIR-FRAP (Fig. 1a) to selectively monitor the kinetics of repopulation of the membrane and of the subcellular structures involved. Comparison of the total fluorescence intensity before and after the high-intensity TIR illumination step revealed that TRPV2-GFP fluorescence detected in the TIRF mode was almost completely annihilated, whereas TRPV2-GFP fluorescence measured using in epifluorescence excitation was reduced by only approximately 40% (Fig. 1b,d). Similar results were obtained for TRPM4-GFP (Fig. 1c,e). These results demonstrate that the high-intensity TIR illumination step was effective in bleaching a restricted part of the cells close to the glass coverslip, while leaving fluorescence in the remaining of the cell largely intact.

TIR-FRAP reveals distinct modes of TRP channel recovery. Following the bleaching step, we first analyzed the recovery of global GFP fluorescence in the TIRF field as an index of the rate of movement of the TRP channels from non-bleached parts of the cell towards the bleached perimembrane area (Fig. 2). In the case of TRPV2-GFP, recovery of global fluorescence in the TIRF field could be well described using a single exponential time constant (τ) 88.75 $\pm$ 4.9 s, reaching a maximal recovery of 45 $\pm$ 5%

(Fig. 2c). Global TRPM4-GFP recovered faster (τ = 33.3 $\pm$ 2.7 s) to 48 $\pm$ 8% of the normalized pre-bleach fluorescence (Fig. 2d).

Although the extent of recovery was similar for both TRP channels, we observed clear differences in the pattern of fluorescence recovery. In particular, recovery of TRPV2-GFP appeared to occur from the sides towards the center, whereas recovery of TRPM4-GFP fluorescence appeared more homogenous over the entire footprint of the cell. To analyze this difference in more detail, we measured fluorescence recovery in twenty concentric and equally spaced bands covering the cell footprint from center to the periphery (band 1 being at the center and 20 being just beyond the outside rim of the foot print) (Fig. 3a). Fig. 3b,d show representative time courses of normalized fluorescence recovery in band 2 and 18 for TRPV2-GFP and TRPM4-GFP, respectively, together with the recovery time course of the entire footprint. Whereas for TRPM4 the three time courses overlap, the recovery of TRPV2 in the central parts of the footprint clearly lagged behind that at the border. This was quantified by determining the exponential time constants of the fluorescence recovery in the different bands, showing increasing values towards the center of the cell for TRPV2 (Fig. 3c) but not for TRPM4 (Fig. 3e).

The fluorescence recovery pattern of TRPV2-GFP is consistent with a process of recovery where channels located in the plasma membrane outside the bleached areas slide into the footprint via lateral diffusion. Assuming that bleach intensity is uniform over the footprint of the cell, that fluorescence recovery occurs exclusively by lateral diffusion from non-bleached areas of the plasma membrane (i.e. the side and upper part of the plasma membrane, beyond the evanescent wave), and that the bleached area is circular, then the diffusion coefficient D can be estimated from the recovery time constant for the center of the cell according to:

$$D = a^2/4\tau \qquad (1)$$

where a is the radius of the bleached area[24,25]. To reduce errors due to the fact that the bleached area was never a perfect circle, we restricted
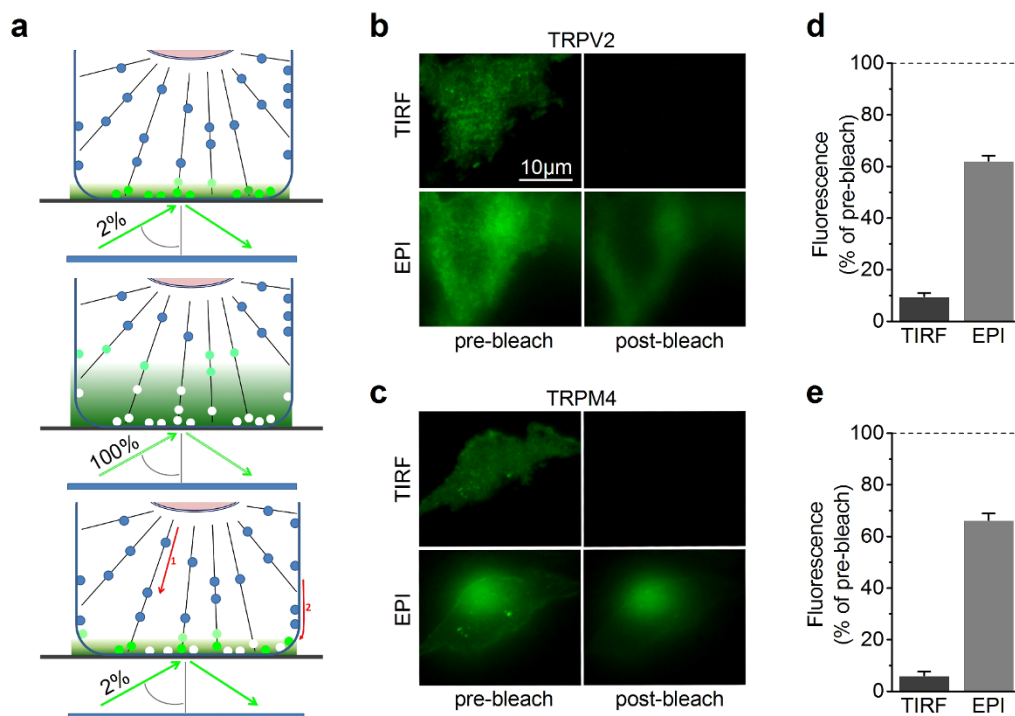

Figure 1 | Scheme of the TIR-FRAP experiment. (a) Low intensity (2% of maximal laser power) TIRF illumination was applied during both the pre-bleach (top) and post-bleach-recovery phase (bottom). During the bleaching phase, the TIRF angle was maintained, but laser power was increased to 100%. (b,c) Epifluorescence and TIRF micrographs of TRPV2-GFP and TRPM4-GFP transfected in HEK293 cells before and immediately following bleaching. (d,e) Fluorescence intensities in epifluorescence and TIRF normalized to the respective pre-bleach intensities.
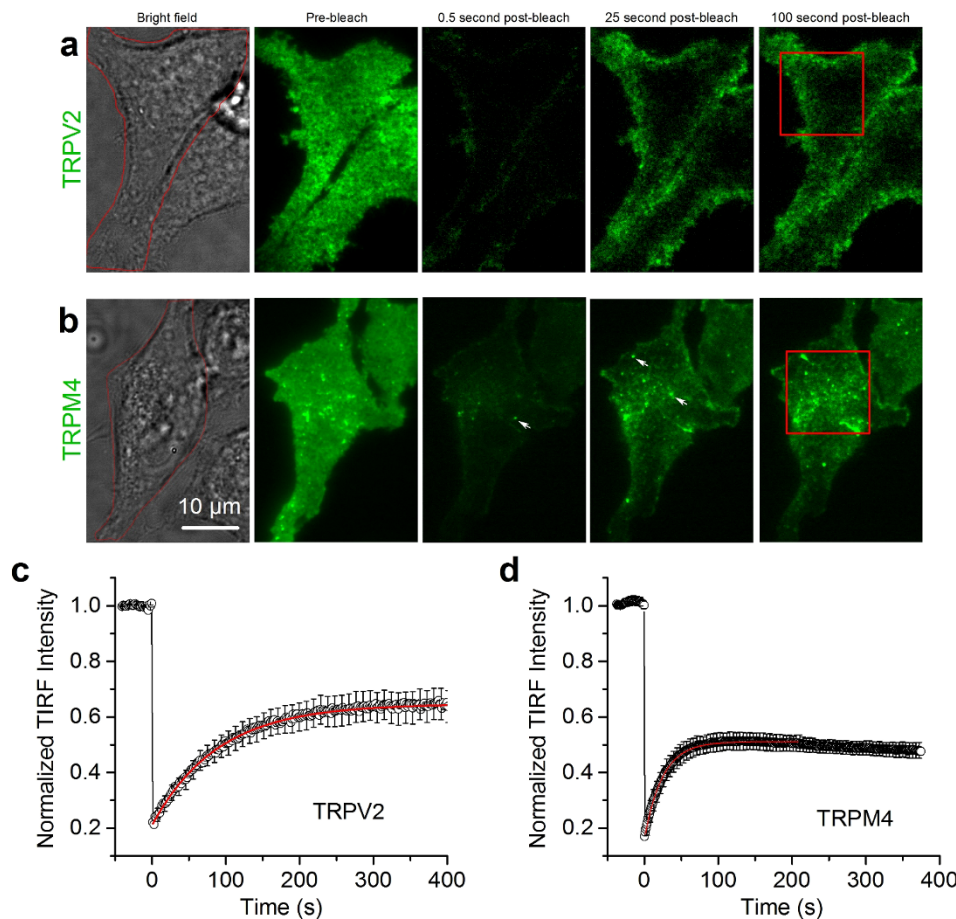
Figure 2 | Global fluorescence recovery in TIR-FRAP. (a,b) Brightfield (left) and TIRF micrographs at the indicate time points of HEK293 cells expressing TRPV2-GFP and TRPM4-GFP. The red squares depict the regions shown in movies 1 and 2. Arrows indicate incoming and subsequently fusing TRPM4-GFP-containing vesicles. (c,d) Average time course of normalized fluorescence during TIR-FRAP experiments for TRPV2-GFP and TRPM4-GFP. Time 0 corresponds to the start of the post-bleach recovery.

our analysis to cells with a semi-circular footprint (circularity >0.6). This analysis yielded a mean diffusion coefficient for TRPV2-GFP (D_{TRPV2}) of 0.30 ± 0.04 μm²/s (n = 8).

Full fusion of TRPM4-carrying vesicles. In contrast to TRPV2, the time constants for recovery of TRPM4-GFP fluorescence were relatively constant in the different bands, suggesting that recovery mainly occurs from inside the cell towards the plasma membrane rather than through lateral diffusion. Indeed, when resident fluorescence from the membrane and sub-membrane zone was absent because of the high-intensity TIR illumination step, we observed abundant punctate structures that approached the plasma membrane and subsequently fused with the membrane (Supplementary movies S3 and S4).

Fig. 4a shows successive frames of a small subregion of the foot-print of a TRPM4-GFP-expressing cell, zooming in on an area where a single vesicle appears and fuses with the plasma membrane. Subtraction of average images before appearance of the vesicle allowed visualization of the fusion event in isolation (Fig. 4b,c; Supplementary movie S5). Four distinct stages could be identified: (1) vesicle approach, observed as the appearance of punctate fluor-escent spot that gradually increases in intensity as it progresses in the evanescent field; (2) vesicle lingering, observed as a period of static fluorescence of the punctate spot; (3) vesicle fusion, observed as a sudden rapid increase in fluorescence immediately followed by (4) a rapid spreading of the fluorescence due to lateral spread of the TRPM4-GFP molecules in the plasma membrane.

Based on the point spread function determined from the fluor-escence signal of beads with known diameter, we calculated the radius (r_v) of isolated fusing vesicles, yielding a mean value of 96 ± 3 nm (n = 15). Moreover, taking into account the decay length constant of the evanescent wave and assuming that the entire vesicle membrane becomes aligned in the z-direction with the plasma mem-brane following fusion (Fig. 4d), we derived the following mathemat-ical relation between the fluorescence intensity contributed by a single vesicle (I) with its edge at a distance z_v from the plasma mem-brane during vesicle approach and lingering:

$$z_v = -d \times \left(\ln\left(\frac{I(z_v)}{I_{max}} \times \frac{2r_v}{d} \right) - \ln\left(1 - e^{-\frac{2r_v}{d}} \right) \right) \qquad (2)$$

where d is the decay constant of the evanescent wave (80 nm) and I_{max} the maximal fluorescence following full fusion (see methods for derivation of equation 2). Based on equation 2 we calculated z_v in function of time for multiple clearly resolvable fusion events (Fig. 4e). This analysis yielded that TRPM4-GFP-containing vesicles approach the plasma membrane from inside the cell with a speed in the z-direction of 275 ± 25 nm/s (n = 15), and linger during 7.6 ± 1.2 s at a distance of $z_v = 27 ± 5$ nm from the membrane before fusion.

To analyze the speed of lateral TRPM4 diffusion in the plasma membrane following fusion, we determined the two-dimensional root-mean-square (rms) displacement of TRPM4-GFP fluorescence from the site of fusion (Fig. 4f). The time course of the increase in rms (Δrms) in function of time post fusion was fitted to the two-dimen-sional diffusion function:

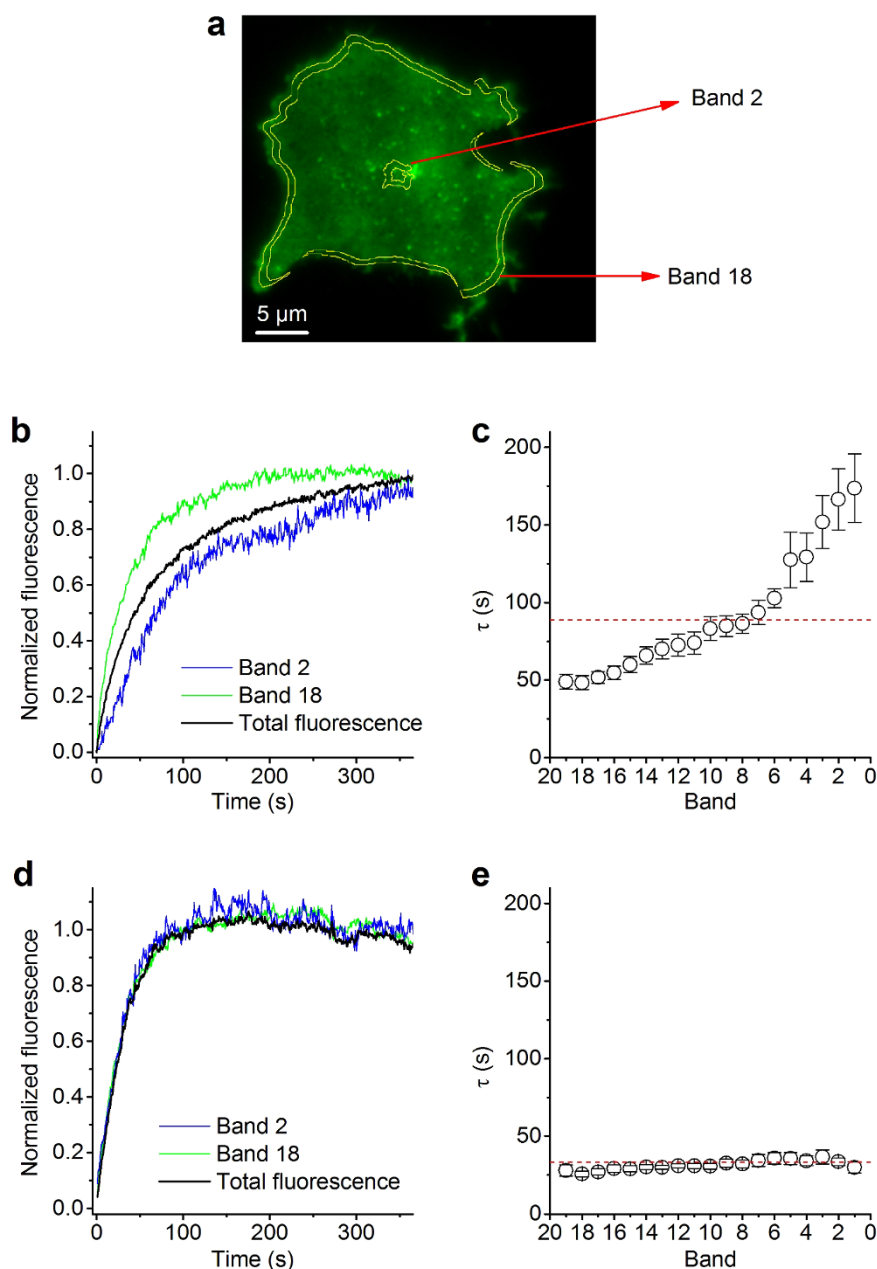$$\Delta rms = \sqrt{4Dt} \qquad (3)$$

Figure 3 | Spatio-temporal analysis of post-bleach recovery. (a) TIRF micrograph showing the footprint of a TRPM4-GFP-expressing cell. Superimposed are bands 2 and 18 of the 20 concentric, equally shaped and equidistant bands that were used to analyze the spatio-temporal aspects of fluorescence recovery. (b) Normalized TRPV2-GFP fluorescence following bleaching in a central and peripheral band, along with the global fluorescence of the entire footprint. (c) Exponential time constants for the recovery of fluorescence in the different bands. (d,e) Same as (b,c) but for cells expressing TRPM4-GFP.

yielding a value for D_{TRPM4} of 0.102 ± 0.014 µm²/s (n = 15). Note that this value is 5-fold higher than previously determined for TRPM4[20]. This may reflect that this previous study used confocal FRAP, and thus measured both plasma membrane and intracellular TRPM4, whereas our analysis uniquely reflects the spread of TRPM4 in the plasma membrane following fusion.

Discussion

In this study, we have used TIR-FRAP to visualize the perimembrane movement of TRPM4 and TRPV2 upon expression in HEK293 cells. Our results indicate that these channels exhibit quite different dynamics in the TIRF field. Within the seconds-to-minutes time scale of our experiments, we were unable to detect vesicular transport of TRPV2 toward the membrane, and the fluorescence recovery pattern could be fully explained by lateral diffusion within the plasma membrane from non-bleached plasma membrane areas outside the TIRF field. Even when assessed at different time points between 4 and 48 hours after transfection, TRPV2 fluorescence evenly covered the entire footprint of the cell, and clear vesicular structures or fusion events were never observed. These results suggest that incorporation of TRPV2 in the plasma membrane occurs via vesicular structures that are too small or too rare to be clearly resolved under our experimental conditions. In contrast, we consistently observed active constitutive transport and membrane fusion of TRPM4-containing vesicles. Overall, these results point towards an important qualitative difference in the processes that underlie incorporation of TRPM4 and TRPV2 in the plasma membrane.
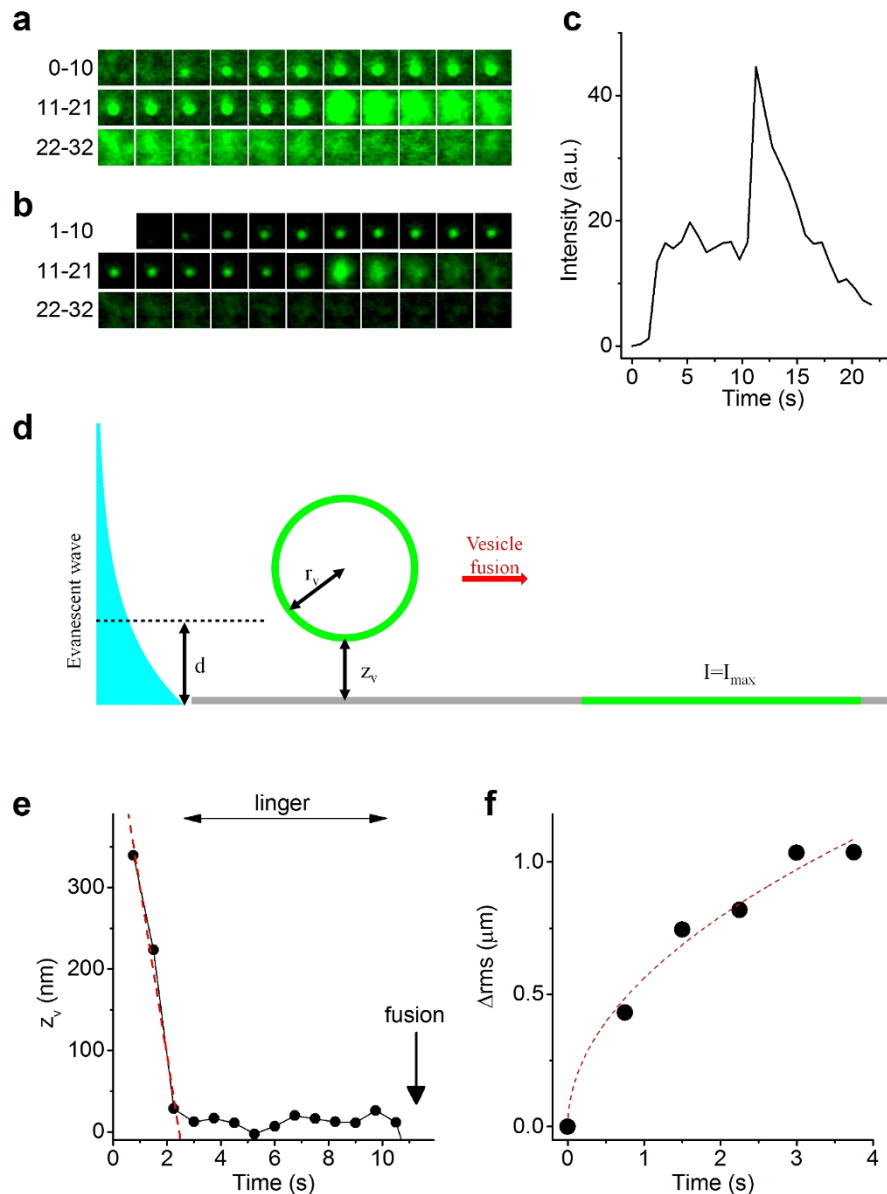
Figure 4 | Full fusion of TRPM4-containing vesicles. (a) Successive 1.2 μm×1.2 μm frames at 750-ms interval of a fusion event of a TRPM4-GFP carrying vesicle. (b) Same as (a), but after subtraction of frame 0. (c) Time course of background-subtracted fluorescence. (d) Cartoon showing a fluorescent vesicle within the evanescent wave, and after full collapse with the plasma membrane. (e) Time course of z_v showing vesicle approach and lingering before fusion. Red dotted line represents a linear fit, yielding a speed in the *z*-direction of 207 nm/s. (f) Increase in *rms* after fusion. Red dotted trace represents a fit of equation 3, yielding D=0.078 μm²/s. Analyses in (c–f) are all for the fusion example shown in (a,b).

Although TIRF microscopy has been used before to demonstrate vesicular movement of TRPM8, TRPC5 and TRPV5 towards the membrane[9,11,17], full fusion of vesicles containing these channels has never been observed. Instead, it was proposed that vesicles containing TRPM8, TRPC5 and TRPV5 interact with the plasma membrane through a process termed "kiss and linger", in which these channels access the extracellular medium via a reversible fusion pore but remain trapped within the non-collapsed vesicle[11,17]. Our results with TRPM4 show for the first time the full fusion of TRP channel-containing vesicles, followed by rapid lateral spreading of the channels within the plasma membrane. Since background membrane fluorescence was low thanks to the preceding TIR-FRAP bleaching, we were able resolve and quantify in detail the approach, lingering and fusion of these vesicles, which had a typical diameter of ∼200 nm.

TRPM4-containing vesicles approached the plasma membrane at a maximal speed of ∼275 nm/s, a value in between published approach velocities for large dense-core vesicles in chromaffin cells (∼140 nm/s)[26] or smaller synaptic vesicles (∼800 nm/s) at neuronal synapses[27], and are in the expected range for vesicle transport along microtubular tracts. Before fusion, the TRPM4-containing vesicles lingered for on average 7.6 seconds at an estimated distance of ∼25 nm from the membrane. This distance was estimated based on the assumption that the plasma membrane where the vesicle fuses remains fully flat during the entire fusion process, and may thus represent a slight overestimation of the actual minimal distance between vesicle and plasma membrane. We therefore speculate that the lingering period represents the process of vesicle docking/tethering at the membrane and the formation of fusion complexes before actual vesicle fusion[28].

The diffusion coefficients we obtained for TRPM4 and TRPV2 in the plasma membrane are comparable to those obtained for other mobile membrane channels such as $K_V2.1$ (0.06 μm²/s)[29] and extra-synaptic AMPA receptors (0.45 μm²/s)[30] or for rhodopsin in rod membranes (0.4 μm²/s)[31], but several others of magnitude higher

than those obtained for membrane proteins whose lateral movement is restricted, such as synaptic AMPA receptors (<0.007 μm^2/s)[30] or immobile GABA receptors (0.0003 μm^2/s)[32]. This suggests that, at least in HEK293 cells, TRPV2 and TRPM4 have high lateral mobility and distribute evenly in the plasma membrane[33].

Overall, our study demonstrates the usefulness of TIR-FRAP to visualize and quantify the perimembrane dynamics and turnover of TRP channels. Our results reveal that, on a seconds to minutes time scale, TRPM4 and TRPV2 exhibit fundamentally different dynamics. Most importantly, we show that, in contrast to the "kiss and linger" process previously described for vesicles transporting TRPM8, TRPC5 and TRPV5, TRPM4-carrying vesicles undergo full fusion. Since altered channel trafficking has been put forward as a main mechanism underlying cardiac conduction diseases in patients with mutations in the TRPM4 gene[21,34], this work may represent an interesting paradigm for further research on the molecular and cellular basis of these diseases.

Methods

HEK293 cell culture. Human embryonic kidney cells (HEK293) were grown in Dulbecco's modified Eagle's medium (DMEM) that contained 10% (v/v) human serum, 2 mM L-glutamine, 2 units/ml penicillin and 2 mg/ml streptomycin (Invitrogen) at 37°C in a humidity-controlled incubator with 10% CO_2. HEK293 cells were transiently transfected with cDNA encoding TRPM4-GFP (in the pCAGGSM2 vector) or TRPV2-GFP (in the pCiNeo vector) using Mirus 293 Transfection Reagent (Mirus Corporation, Madison, USA). For most experiments, cells were kept in the transfection medium for 4 h, and subsequently reseeded on poly-L-lysine-coated 25-mm glass coverslips with thickness of 0.16–0,19 mm (Gerhard Menzel GmbH, Germany). Thereafter, cells were kept under the same culture conditions for an additional 12 h, allowing optimal attachment of the cells to the glass coverslip, and resulting in a total of 16 h between transfection and TIRF measurement. For the experiments shown in Supplementary Figure S1, incubation times were adjusted, such that measurements were made after between 4 and 72 hours of total transfection time.

TIRF Microscopy. Experiments were performed at 25°C and using an extracellular solution that contained (in mM): 150 NaCl, 6 KCl, 2 MgCl$_2$, 2 CaCl$_2$, 10 HEPES (pH 7.4). We used a through-the-lens TIRF system that was built around an inverted Zeiss Axio Observer.Z1 microscope equipped with a 100× oil objective with numerical aperture of 1.45 and a Hamamatsu Orca-R^2 camera. Fluorescence excitation was performed using a 488-nm laser at 2% of its maximal power, with an incident angle of 68°, resulting in an evanescent wave with an expected decay length constant of 80 nm. For epifluorescence images, the incident angle was changed to 0°. Time series of images at 750-ms or 1600-ms intervals were recorded. The bleaching protocol consisted of 50 exposure sequences with the 488-nm laser set at 100% of its maximal power. Constant focus was guaranteed by use of the Zeiss Definite Focus module.

Data analysis. Microscopy images were analyzed using home-written routines in ImageJ. Further data analysis was performed using Origin 8 (OriginLab Corporation, USA). Group data are shown as mean ± s.e.m. Fluorescence recovery time courses were corrected for ongoing bleaching, where the frame-to-frame bleaching rate was determined before the high-intensity TIR illumination step and assumed to be constant.

To obtain equation 2, we assumed spherical vesicles with a uniform density of fluorescent molecules in their membranes. The fluorescent signal per surface area (F) decays in the z direction according to

$$F = F_{max} \cdot e^{-\frac{z}{d}} \qquad (4)$$

where F_{max} is the fluorescence per surface area at z = 0. Upon full collapse with a flat plasma membrane, the fluorescent signal of a single vesicle reaches a maximum given by:

$$I_{max} = 4\pi r_v^2 \cdot F_{max}. \qquad (5)$$

Before fusion, the total fluorescent signal of a vesicle in the decaying evanescent wave can be obtained by integrating F over the surface of the vesicle, which is given by:

$$I(z_v) = \int_{\gamma=0}^{\pi} F_{max} e^{-\frac{z_v + r_v(1-\cos\gamma)}{d}} \cdot 2 \cdot r_v^2 \cdot \sin\gamma \cdot d\gamma \qquad (6)$$

where the integration variable γ is the angular distance from the vesicle pole closest to the membrane. Dividing the result of equation 6 by equation 5 yields:

$$\frac{I(z_v)}{I_{max}} = \frac{d}{2r_v} e^{-\frac{z_v}{d}} \left(1 - e^{-\frac{2r_v}{d}}\right) \qquad (7)$$

which, upon isolation of z_v, yields equation 2.

1. Flockerzi, V. & Nilius, B. TRPs: truly remarkable proteins. *Handb Exp Pharmacol* **222**, 1–12, doi:10.1007/978-3-642-54215-2_1 (2014).

2. Gees, M., Owsianik, G., Nilius, B. & Voets, T. TRP channels. *Compr Physiol* **2**, 563–608, doi:10.1002/cphy.c110026 (2012).

3. Clapham, D. E. TRP channels as cellular sensors. *Nature* **426**, 517–524, doi:10.1038/nature02196nature02196 (2003).

4. Nilius, B. & Szallasi, A. Transient receptor potential channels as drug targets: from the science of basic research to the art of medicine. *Pharmacol Rev* **66**, 676–814, doi:66/3/67610.1124/pr.113.008268 (2014).

5. Vriens, J., Nilius, B. & Voets, T. Peripheral thermosensation in mammals. *Nat Rev Neurosci* **15**, 573–589, doi:nrn3784 10.1038/nrn3784 (2014).

6. Toro, C. A., Arias, L. A. & Brauchi, S. Sub-cellular distribution and translocation of TRP channels. *Curr Pharm Biotechnol* **12**, 12–23, doi:BSP/CPB/E-Pub/0002-12-1 (2011).

7. Ambudkar, I. S. Trafficking of TRP channels: determinants of channel function. *Handb Exp Pharmacol* **179**, 541–557, doi:10.1007/978-3-540-34891-7_32 (2007).

8. Cayouette, S. & Boulay, G. Intracellular trafficking of TRP channels. *Cell Calcium* **42**, 225–232, doi:10.1016/j.ceca.2007.01.014 (2007).

9. Bezzerides, V. J., Ramsey, I. S., Kotecha, S., Greka, A. & Clapham, D. E. Rapid vesicular translocation and insertion of TRP channels. *Nat Cell Biol* **6**, 709–720, doi:10.1038/ncb1150 (2004).

10. Cheng, H. *et al.* TRPM4 controls insulin secretion in pancreatic beta-cells. *Cell Calcium* **41**, 51–61, doi:10.1016/j.ceca.2006.04.032 (2007).

11. Lambers, T. T. *et al.* Extracellular pH dynamically controls cell surface delivery of functional TRPV5 channels. *Mol Cell Biol* **27**, 1486–1494, doi:MCB.01468-06 10.1128/MCB.01468-06 (2007).

12. Schmidt, M., Dubin, A. E., Petrus, M. J., Earley, T. J. & Patapoutian, A. Nociceptive signals induce trafficking of TRPA1 to the plasma membrane. *Neuron* **64**, 498–509, doi:S0896-6273(09)00741-7 10.1016/j.neuron.2009.09.030 (2009).

13. Oancea, E., Wolfe, J. T. & Clapham, D. E. Functional TRPM7 channels accumulate at the plasma membrane in response to fluid flow. *Circ Res* **98**, 245–253, doi:01.RES.0000200179.29375.cc 10.1161/01.RES.0000200179.29375.cc (2006).

14. Steyer, J. A. & Almers, W. A real-time view of life within 100 nm of the plasma membrane. *Nat Rev Mol Cell Biol* **2**, 268–275, doi:10.1038/35067069 (2001).

15. Mattheyses, A. L., Simon, S. M. & Rappoport, J. Z. Imaging with total internal reflection fluorescence microscopy for the cell biologist. *J Cell Sci* **123**, 3621–3628, doi:10.1242/jcs.056218 (2010).

16. Axelrod, D. Total internal reflection fluorescence microscopy in cell biology. *Traffic* **2**, 764–774 (2001).

17. Veliz, L. A. *et al.* Near-membrane dynamics and capture of TRPM8 channels within transient confinement domains. *PLoS One* **5**, e13290, doi:10.1371/journal.pone.0013290 (2010).

18. Pryazhnikov, E., Fayuk, D., Niittykoski, M., Giniatullin, R. & Khiroug, L. Unusually Strong Temperature Dependence of P2X3 Receptor Traffic to the Plasma Membrane. *Front Cell Neurosci* **5**, 27, doi:10.3389/fncel.2011.00027 (2011).

19. Pochynyuk, O., Staruschenko, A., Bugaj, V., Lagrange, L. & Stockand, J. D. Quantifying RhoA facilitated trafficking of the epithelial Na+ channel toward the plasma membrane with total internal reflection fluorescence-fluorescence recovery after photobleaching. *J Biol Chem* **282**, 14576–14585, doi:10.1074/jbc.M701348200 (2007).

20. Crnich, R. *et al.* Vasoconstriction resulting from dynamic membrane trafficking of TRPM4 in vascular smooth muscle cells. *Am J Physiol Cell Physiol* **299**, C682–694, doi:10.1152/ajpcell.00101.2010 (2010).

21. Kruse, M. *et al.* Impaired endocytosis of the ion channel TRPM4 is associated with human progressive familial heart block type I. *J Clin Invest* **119**, 2737–2744, doi:10.1172/JCI38292 (2009).

22. Kanzaki, M. *et al.* Translocation of a calcium-permeable cation channel induced by insulin-like growth factor-I. *Nat Cell Biol* **1**, 165–170, doi:10.1038/11086 (1999).

23. Kojima, I. & Nagasawa, M. Trpv2. *Handb Exp Pharmacol* **222**, 247–272, doi:10.1007/978-3-642-54215-2_10 (2014).

24. Kapitza, H. G., McGregor, G. & Jacobson, K. A. Direct measurement of lateral transport in membranes by using time-resolved spatial photometry. *Proc Natl Acad Sci U S A* **82**, 4122–4126 (1985).

25. Chen, Y., Lagerholm, B. C., Yang, B. & Jacobson, K. Methods to measure the lateral diffusion of membrane lipids and proteins. *Methods* **39**, 147–153, doi:S1046-2023(06)00078-8 10.1016/j.ymeth.2006.05.008 (2006).

26. Steyer, J. A. & Almers, W. Tracking single secretory granules in live chromaffin cells by evanescent-field fluorescence microscopy. *Biophys J* **76**, 2262–2271, doi:10.1016/S0006-3495(99)77382-0 (1999).

27. Zenisek, D., Steyer, J. A. & Almers, W. Transport, capture and exocytosis of single synaptic vesicles at active zones. *Nature* **406**, 849–854, doi:10.1038/35022500 (2000).

28. Toomre, D., Steyer, J. A., Keller, P., Almers, W. & Simons, K. Fusion of constitutive membrane traffic with the cell surface observed by evanescent wave microscopy. *J Cell Biol* **149**, 33–40 (2000).

29. Tamkun, M. M., O'Connell, K. M. & Rolig, A. S. A cytoskeletal-based perimeter fence selectively corrals a sub-population of cell surface Kv2.1 channels. *J Cell Sci* **120**, 2413–2423, doi:120/14/2413 10.1242/jcs.007351 (2007).

30. Tardin, C., Cognet, L., Bats, C., Lounis, B. & Choquet, D. Direct imaging of lateral movements of AMPA receptors inside synapses. *EMBO J* **22**, 4656–4665, doi:10.1093/emboj/cdg463 (2003).

31. Wey, C. L., Cone, R. A. & Edidin, M. A. Lateral diffusion of rhodopsin in photoreceptor cells measured by fluorescence photobleaching and recovery. *Biophys J* **33**, 225–232, doi:S0006-3495(81)84883-7 10.1016/S0006-3495(81)84883-7 (1981).

32. Peran, M., Hicks, B. W., Peterson, N. L., Hooper, H. & Salas, R. Lateral mobility and anchoring of recombinant GABAA receptors depend on subunit composition. *Cell Motil Cytoskeleton* **50**, 89–100, doi:10.1002/cm.1043 10.1002/cm.1043 (2001).

33. Jacobson, K. A. *et al*. Cellular determinants of the lateral mobility of neural cell adhesion molecules. *Biochim Biophys Acta* **1330**, 138–144 (1997).

34. Liu, H. *et al*. Gain-of-function mutations in TRPM4 cause autosomal dominant isolated cardiac conduction disease. *Circ Cardiovasc Genet* **3**, 374–385, doi:10.1161/CIRCGENETICS.109.930867 (2010).

Acknowledgments

Author contributions

D.G. and T.V. designed experiments. D.G. performed experiments. A.S and T.V. developed and programmed analytical tools. D.G., A.S and T.V. analyzed data. D.G. and T.V. wrote the manuscript. All authors reviewed the manuscript. T.V. supervised the project.

Additional information

Supplementary information accompanies this paper at http://www.nature.com/scientificreports

Competing financial interests: The authors declare no competing financial interests.

How to cite this article: Ghosh, D., Segal, A. & Voets, T. Distinct modes of perimembrane TRP channel turnover revealed by TIR-FRAP. *Sci. Rep.* **4**, 7111; DOI:10.1038/srep07111 (2014).